Retrieval of aerosol optical thickness from NOAA/AVHRR data on the sea and land areas

○ K. Asakuma, S. Otsutsumi, M. Yabuki, T. Kubota, H. Kuze, and N. Takeuchi
Center for Environmental Remote Sensing, Chiba University
1-33 Yayoi-cho, Inage-ku, Chiba, 263-8522, Japan
asakuma@ceres.cr.chiba-u.ac.jp

Abstract:
We present a retrieval algorithm of aerosol optical thickness over the land area. This algorithm is based on the dark-target approach combined with the texture analysis. In the first part of the algorithm, we employ the 6S code to calculate the relevant radiance components. The aerosol optical thickness is retrieved over the sea surface assuming a surface reflectance of 2 % with typical aerosol models in the 6S code (e.g. Maritime, Urban and Continental). In addition, we present a "Kanto" aerosol model on the basis of the ground measurements conducted at 11 sites on the Kanto plain during December 22-24, 1997. In this model, chemical composition data are used to derive the single scattering albedo and the asymmetry parameter. These optical parameters are useful to improve the accuracy of the radiation calculation with the 6S code. This method is applied to several sites arbitrary chosen on the sea area, and by two-dimensional linear interpolation, we obtain a "τ-image" over the land area. In the second part, a difference image is calculated between an actual satellite image (turbid image, NOAA AVHRR channel 1 on December 1, 1997) and a clear image that is obtained by applying the atmospheric correction to a satellite image (December 15, 1997). In the last part, the atmospheric features included in the difference image are analyzed by the texture analysis. For each area that includes both land and sea surfaces, and is categorized into a texel (i.e. its atmospheric feature is considered to be uniform), the optical thickness of the land area is assumed to be the same as that over the sea area. As a whole, the present method makes it possible to extend the method of analyzing atmospheric conditions from satellite data to the land surfaces that are surrounded by water areas.

1. Introduction

In order to derive precise surface reflectance from satellite image data in the visible and near-infrared bands, it is required to conduct the atmospheric correction which serves to remove the effects of molecular and aerosol scattering [1]. Generally the parameters needed in this type of calculation are the values of the optical thickness for molecules and aerosol particles. Thus far, we have studied the atmospheric correction based on a modification of the Richter's two-step algorithm [2, 3]. Since the chemical composition and size distribution of aerosol are quite variable, it is desired to devise some operational techniques to determine the aerosol optical thickness from satellite images themselves. A τ-map that describes the horizontal distribution of aerosol optical thickness could possibly be obtained by interpolating the aerosol optical properties observed at several sites using ground sampling and ground observations by means of instruments such as a sun-photometer and a lidar[4, 5]. Obviously this method could become laborious since it requires simultaneous observations at sufficient number of sites. In contrast, satellite images themselves can provide the instantaneous distribution of aerosol optical thickness in a broad area, once the ground reflectance is given. This approach, however, is hardly applicable to land surfaces because of a wide variety of surface conditions such as urban area, forest area, etc. In contrast, the sea surface and vegetation canopy exhibit more or less uniform reflectance, and over such surfaces, it becomes possible to retrieve the aerosol optical thickness by means of radiation transfer calculations. Recently the development of radiation transfer codes such as the 6S [6] has improved the situation, since they are equipped with standardized atmospheric conditions such as typical aerosol models. Moreover, the 6S code allows the user also to define the aerosol size distribution.

In this paper we present an algorithm for deriving the aerosol optical thickness over land areas surrounded by sea (or dark target) areas. Radiation transfer calculations and image processing techniques are combined to analyze the NOAA AVHRR images over the Chiba area. In the demonstration of our algorithm, we make use of the 6S code with its standardized aerosol models. In addition, we describe a method to determine aerosol optical quantities from their chemical properties acquired by ground sampling.

2. Algorithms

2.1 Radiance components detected by a satellite sensor

In the visible and near-infrared bands, a satellite sensor detects the radiance that is affected by the atmospheric absorption and scattering. The radiance received by a sensor is expressed as :

$$L_{\text{total}}^{\text{SAT}} = (DN \cdot S + I)\frac{E_s}{100\pi W} \qquad (1)$$

where DN stands for the digital number at each pixel in the satellite image, E_s is the solar irradiance at the top of the atmosphere, W is the band width, and S and I are the calibration constants of the satellite sensor. Figure 1 shows the radiance components detected by a satellite sensor. The 6S code computes the following six components : 1) L_{tar} : The radiance due to the target pixel L_{tar} includes the three components of L_{gd}, L_{gi}, and L_{gi}. 2) L_{env} : The "environmental" radiance arising from the contigu-

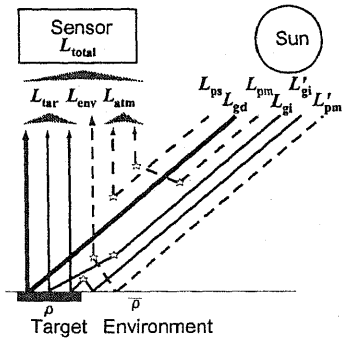

Fig. 1: Radiance components detected by a satellite sensor.

ous pixels. 3) $L_{\rm atm}$: The path radiance originating from the single and multiple atmospheric scattering.

The 6S code does not provide the directly ground reflected component, $L_{\rm gd}$. Alternatively, we use the following equation to obtain this component, which is denoted as $L_{\rm gd}^{\rm RTC}$:

$$L_{\rm gd}^{\rm RTC} = \frac{1}{\pi}\int E_s(\lambda)T_g^{\lambda}(\theta_s)\mu_s e^{-\tau/\mu_s}\rho e^{-\tau/\mu_v}d\lambda. \quad (2)$$

Here τ_{550} stands for the aerosol optical thickness at 550nm, used as an input parameter in the 6S code. Now the directly ground-reflected radiance observed by the satellite sensor, $L_{\rm gd}^{\rm SAT}$, is expressed as a function of τ_{550}:

$$L_{\rm gd}^{\rm SAT} = L_{\rm total}^{\rm SAT} - L^{'}(\tau_{550}), \quad (3)$$

$$L^{'}(\tau_{550}) = L_{\rm total} - L_{\rm gd}^{\rm RTC}, \quad (4)$$

$$L_{\rm total} = L_{\rm atm} + L_{\rm env} + L_{\rm tar} \quad (5)$$

where $L_{\rm total}^{\rm SAT}$ is the radiance received by the AVHRR sensor (channel 1) obtained with Eq.(1), and $L^{'}(\tau_{550})$ the total path radiance at 550 nm: this path radiance is a function of τ_{550} alone when the ground reflectance ρ is assumed to be 0.

2.2 Construction of Kanto aerosol models from the chemical properties

Aerosol particles are emitted from diverse origins and suspended in the air incessantly changing their size and composition[7]. Although there exist numerous ways to classify the aerosol composition, primary components are soil and sea salt from natural origin, carbon and heavy metal from artificial sources, and water-solubles such as sulfates and nitrates. In the visible wavelength, particularly important components are elementary carbon and water-soluble particle, both of which effectively absorb visible photons. Moreover, water-soluble particles promote the cloud condensation working as nuclei in the process. In the simple treatment of the global radiative forcing, it is customary to use the ratio between elementary carbon and water-solubles[8]. Also in the 6S code, aerosol optical properties are calculated using this ratio as well as the parameters describing the soil and maritime components.

In the present work, we adopt the method developed by Ota[9]. Namely, it is assumed that in the troposphere aerosol particles consist of six species, *i.e.* elementary carbon (EC), organic carbon (Org), ammonium sulfate ($(NH_4)_2SO_4$), ammonium nitrate (NH_4NO_3), sea salt cation, and soil. The effect of humidity on the particle radius and density of water-soluble particles are incorporated by the Tang's theory. For non water-soluble particles, values of density, radius, and refractive index are assumed to be constant irrespective of the relative humidity.

In the sampling, a low-volume Andersen sampler is used with quartz fiber and poly-flon filters, giving classification of the particle radius in nine classes. Ion and carbonic components are detected by analyzing particles clinging to each filter. These components are divided into the above six species, and for each, the size distribution is determined by fitting the result to a bimodal, lognormal distribution. Since the refractive index of each constituent is available[12], the Mie-calculation gives the extinction coefficient $\sigma_{\rm ext}$, scattering coefficient $\sigma_{\rm sca}$, and scattering phase function $P_i(\theta)$ for each component:

$$\sigma_{\rm ext}^i = \int Q_{\rm ext}^i(r,\widetilde{n})\cdot n_i(r)dr, \quad (6)$$

$$\sigma_{\rm sca}^i = \int Q_{\rm sca}^i(r,\widetilde{n})\cdot n_i(r)dr, \quad (7)$$

$$\int P_i(\theta)d\Omega = 4\pi, \quad (8)$$

where $Q_{\rm ext}$ and $Q_{\rm sca}$ are the extinction and scattering cross section, and the suffix $i = [1,2,\cdots,6]$ refers to the aerosol species. For the mixture of the six components, the single scattering albedo ω_0 and the asymmetry factors g are calculated using the sum of $\sigma_{\rm ext}$, $\sigma_{\rm sca}$ and $P_i(\theta)$.

2.3 Determination of τ and construction of τ-MAP

In this paper, we derive the optical thickness from images of AVHRR channel 1 (centered at 630nm). The reflectance of the sea surface is assumed to take a constant value of ρ =0.02. In addition to the radiance components mentioned above, the code yields the aerosol optical thickness which corresponds to the center wavelength of 630 nm, $\tau_{630}^{\rm RTC}$. If the target exhibits the Lambertian reflection, the same optical thickness at 630 nm that the satellite sensor observes can also be calculated from the direct component $L_{\rm gd}^{\rm SAT}$ as

$$\tau_{630}^{\rm SAT} = \frac{-1}{\sec\theta_s + \sec\theta_v}\ln\left(\frac{\pi L_{\rm gd}^{\rm SAT}}{E_s\rho\mu_s\mu_v}\right). \quad (9)$$

Thus, we can determine the "best fit" value of the optical thickness from the condition of $L_{\rm gd}^{\rm SAT} = L_{\rm gd}^{\rm RTC}$.

The calculation is carried out at about 30 pixels in Fig.2, arbitrarily chosen on the sea area around the Chiba prefecture (Boso peninsula surrounded by the Tokyo Bay and the Pacific Ocean). By interpolating the τ_{630} values from the sampling points, we

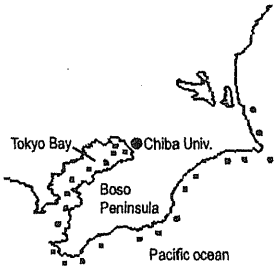

Fig. 2: Sampling points around Boso peninsula.

obtain a τ-map. The two-dimensional interpolation is performed by combining three sampling points ($\triangle$ ABC), linearly interpolating the value on an arbitrary side (e.g. $\overline{\mathrm{BC}}$), and linearly interpolating along the lines which connect each sampling point on the chosen side ($\overline{\mathrm{BC}}$) with the residual point of the triangle (A).

For modification of the τ-map, we make use of a classification technique based on the texture analysis. The method is applied to an image obtained by subtracting a "clear" image from an actual "turbid" satellite image. This difference image is thought to involve the main feature of the atmosphere involved in the test image. The actual calculation of the difference image is conducted by converting the radiance values of AVHRR channel 1 into the reflectance values. The difference between the test image reflectance ρ_{t}^* and the reference image reflectance ρ_{c}^* is evaluated by means of the following parameter dif:

$$dif = (\rho_{\mathrm{t}}^* - \rho_{\mathrm{c}}^*)/(\rho_{\mathrm{t}}^* + \rho_{\mathrm{c}}^*). \qquad (10)$$

The texture analysis is carried out to look for regions that are characterized by uniform conditions of the atmosphere [10]. Texture stands for a pattern of radiances which a region exhibits in an image. The actual implementation of the texture analysis generally relies on the co-occurrence probability matrix, $P_{\mathrm{c}}(k,l)_{r\theta}$. This describes the probability that when the distance r and the angle θ between two pixels are specified, the combination of their radiance values becomes (k,l).

In order to simplify the calculation, however, here we adopt the gray level difference vector (GLDV) method, in which the difference in the radiance, $n = |k-l|$, is employed rather than the pair of radiance values [11]. As for the textural feature value, we make use of the following normalized parameter derived from the GLDV, $P_{\mathrm{g}}(n)_{r\theta}$:

$$f_{\mathrm{m}}(r,\theta) = \sum_{n=0}^{N_g-1} nP_{\mathrm{g}}(n)_{r\theta}/(N_g-1). \qquad (11)$$

Here N_g denotes the bin number used in the radiance classification, and the function $f_{\mathrm{m}}(r,\theta)$ takes a value between 0 and 1. This function describes the extent of the difference in the maximum and minimum densities in a image: when high similarity is present among neighboring pixels, $f_{\mathrm{m}}(r,\theta)$ approaches 0.

Using the result of the texture analysis, the interpolation of the τ-map is conducted again. This

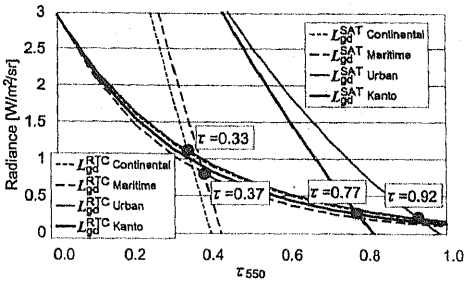

Fig. 3: Relationship between τ_{550}, $L_{\mathrm{gd}}^{\mathrm{SAT}}$ and $L_{\mathrm{gd}}^{\mathrm{RTC}}$ over Tokyo-bay (December 5, 1997).

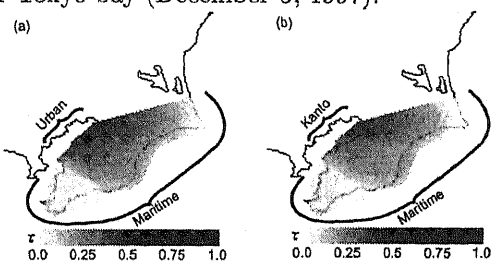

Fig. 4: τ-maps around Chiba (December 5, 1997).

time, when some land and sea areas are included in a region with a uniform condition of the atmosphere (*i.e.* in a texel), the aerosol optical thickness on the sea surface is extended to the land area as well.

3. Results and Conclusions

Figure 3 shows relationship between τ_{550}, $L_{\mathrm{gd}}^{\mathrm{SAT}}$ and $L_{\mathrm{gd}}^{\mathrm{RTC}}$ over Tokyo-bay on December 5, 1997. The typical aerosol models, such as Maritime, Urban and Continental model, and the Kanto model explained in Sec.2.2 are employed with the provided models in 6S code. For each model, the value of τ_{550} is obtained from the condition of $L_{\mathrm{gd}}^{\mathrm{SAT}} = L_{\mathrm{gd}}^{\mathrm{RTC}}$. For acquiring the Kanto aerosol model, simultaneous observations were made at eleven sites to observe chemical properties of aerosol particles during December 22 to December 26, 1997. From this data, we calculate the following four optical parameters that are used as input parameters in the 6S code: the extinction coefficient, single scattering albedo, asymmetry factor, and scattering phase function. We can recognize that result from the Kanto model is close to that from the urban model.

Figure 4 shows τ-maps with combined aerosol model on December 5, 1997. (a) is obtained with the urban aerosol model on the Tokyo-bay side, (b) with Kanto aerosol model. Although the values of τ are different between Fig.4 (a) and (b), the resulting distributions have some characteristics in common: τ is relatively large around the Tokyo Bay, and it tends to decrease toward the east and south directions.

Figure 5 (b) shows the difference image between NOAA AVHRR ch.1 raw image on December 5, 1997 in Fig.5 (a) and its atmospherically corrected image. The correction is made using the Richter's two-step algorithm with the optical thickness values measured

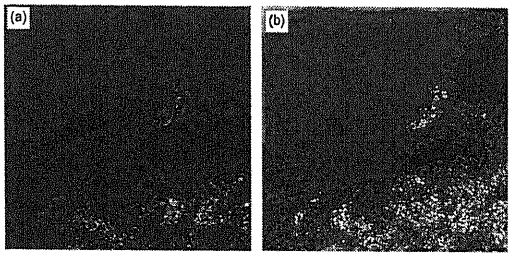

Fig. 5: AVHRR ch. 1 images (December 5, 1997). (a) Raw image and (b) Difference image between the raw image and the atmospherically corrreced image.

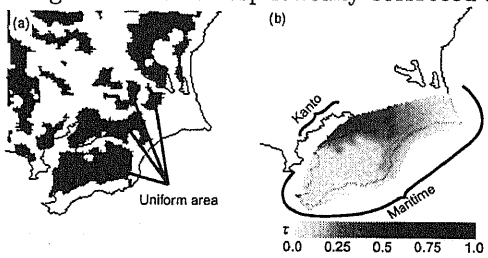

Fig. 6: Result of texture analysis. (a) Uniform atmospheric condition areas obtained from Fig.5 (b) and (b) Modified τ-map with Fig.6 (a).

at Chiba University. Because of the adjacency-effect correction, a trace of the seashore is recognizable in Fig.5 (b). Nevertheless, in this figure as a whole, the influence of the ground reflection has been removed satisfactorily, and the image is mostly contributed from the atmosphere.

The texture analysis is implemented to the difference pixel radiance defined in Eq.(10). and the result is shown in Fig.6 (a). In this figure, black regions indicate that in them, the optical thickness is considered to be uniform. This result is obtained by assuming a texture size of 9×9, $r = 1$, $\theta = 0°$ and $\theta = 90°$. Moreover, we make a logical product of the image with $\theta = 0°$ and $\theta = 90°$, both being converted to binary images with a threshold of $f_{\mathrm{m}}(r, \theta) = 0.3$. In this figure, two regions are discerned that have uniform atmospheric conditions beyond the land/sea borders over the southern part of the Boso peninsula, and three uniform regions are found the northern part of the Boso peninsula.

By supplementing the τ-map in Fig.4 by the texture information in Fig.6 (a), we obtain an improved τ-map as shown in Fig.6 (b). Comparing this figure with Fig.4, it is seen that the region of relatively large τ becomes more limited around the city area. At the same time, the region with smaller τ near the entrance of the bay becomes more extended toward the inland.

In this work, it has been shown that for a land surface surrounded by water areas (or more generally, dark areas), the combination of dark target method and the texture analysis provides a possibility to derive the distribution of aerosol optical thickness from satellite data. A set of reference (atmosphercally corrected) images and aerosol database with the information on the seasonal variations would be particularly beneficial for this purpose. On the basis of a campaign measurement of the aerosol chemical composition, we have also shown that optical information such as the extinction coefficient, scattering coefficient, and scattering phase function are obtainable through the Mie-scattering calculation. These parameters provide a basis for the accurate aerosol model, leading to determination of the aerosol optical thickness map from satellite data over the relevant area.

References

[1] Y. J. Kaufman and C. Sendra : Algorithm for automatic atmosperic corrections to visible and near-IR satellite imagery, Int. J. Remotesensing, 9, 1,357-1,381, 1998

[2] R. Richter : A fast atmospheric correction algorithm applied to Landsat TM image, Int. J. Remotesensing, 11, 159-166, 1990

[3] M. Minomura, J. Ru, H. Kuze and N. Takeuchi : Atomospheric correction of satellile data using Multi-Wavelemgth Lidar data with MODTRAN 3 Code, Adv. Spase Res., 25, 1,033-1,036, 2000

[4] H. Ouaidrari and E. F. Vermote : Operational atomospheric correction of Landsat TM Data, Remote Sens. Env., 70, 4-15, 1999

[5] M. Yabuki : Optical properties of the atmospheric aerosols derived from the lidar measurement and aerosol sampling, Master thesis (in Japanese), Chiba Univ., 2000

[6] E. F. Vermote, D. Tanre, J. Deuze, M. Herman and J. Morcrette : Second simulation of the satellite signal in the solar spectrum, 6S ; An overview, IEEE Trans. on Geosc. and Remote Sens., 35, 675-686, 1997

[7] G. Hanel : Single scattering albedo, asymmetry parameter, apparent refractive index, and apparent soot content of dry particles Appl. Opt., 27, 2,287-2,295, 1988

[8] I. Schult, J. Feichter and W. F. Cooke : Effect of black carbon and sulfate aerosols on the global radiation budget J. Geoph. Res., 102, 30,107-30,117, 1997

[9] S. Ohta, M. Hori, N. Murao, S. Yamagata and K. Gast : Chemical and optical properties of lower tropospheric aerosols measured at Mt. Lemmon in Arizona, J. Global Environ. Engineer., 2, 66-78, 1996

[10] K. S. Kuo and R. M. Welch : Structural and textural characteristics of cirrus clouds observed using high spatial resolution LANDSAT imagery, J. Appl. Meteorol, 27, 1,242-1,260 1988

[11] S. Christopher, D. Kliche, C. Joyce and R. M. Welch : First estimates of the radiative forcing of areosols generated from biomass burning using satellite data, J. Geoph. Res., 101, 21,265-21,273, 1996

[12] A preliminary cloudless standard atmosphere for radiation computation, World Climate Programme; WCP-112, World Meteorological Organization, 1986